ROYAL SOCIETY OF CHEMISTRY

Green Chemistry

Stabilized Fe$_3$O$_4$ magnetic nanoparticles into nanopores of modified montmorillonite clay: A highly efficient catalyst for Baeyer-Villiger oxidation under solvent free condition

SCHOLARONE™
Manuscripts

Stabilized Fe_3O_4 magnetic nanoparticles into nanopores of modified montmorillonite clay: A highly efficient catalyst for Baeyer-Villiger oxidation under solvent free condition

Pallab Kumar Saikia, Podma Pollov Sarmah, Bibek Jyoti Borah, Lakshi Saikia, Kokil Saikia, Dipak Kumar Dutta[*]

Materials Science Division, CSIR-North East Institute of Science and Technology, Jorhat 785006, Assam, India, Fax: (+)91 376 2370011, E-mail: dutta_dk@rrljorhat.res.in

Abstract

In-situ generation of Fe_3O_4 magnetic nanoparticles (Fe_3O_4@AT-mont.) into the nanopores of modified montmorillonite (AT-mont.) clay has been carried out. Modification of the montmorillonite was done by acid (4M HCl) activation under controlled conditions for generating nanopores, which act as a "host" for the Fe_3O_4 nanoparticles. The synthesized Fe_3O_4@AT-mont.was characterized by PXRD, TEM, SEM-EDX, FTIR, XPS, VSM and Surface Area analysis. The average particle size of Fe_3O_4 nanoparticles was found to be around 10 nm and exhibit face centered cubic (fcc) lattice geometry. Fe_3O_4@AT-mont. showed efficient catalytic activity for Baeyer–Villiger oxidation of various cyclic and aromatic ketones in the presence of hydrogen peroxide as an oxidant at room temperature under solvent free condition and exhibited conversion of up to 98 %. The catalyst was magnetically recovered and recycled up to third run without any significant loss of efficiency.

Keywords: Modified montmorillonite, Fe_3O_4 nanoparticles, Baeyer–Villiger oxidation, Magnetic recovery.

1. Introduction

The development of nano-sized metal and metal oxide particles is intensively pursued because of their unique catalytic property and wide range of applicability. Emergence of efficient catalytic system of nanoparticles in organic synthesis has been a challenge for researchers[1-8]. The nano-catalysts contain highly active surfaces and provide the advantages of high atom efficiency, simplified isolation of products and easy recovery and recyclability of the catalysts[2-5]. However, metal nanoparticles are prone to aggregate during catalytic reactions owing to their high surface energy, which decrease the catalytic efficiency. This problem of aggregation has led to the importance of using various stabilizers or supports[9-11]. The stabilizer/support plays an important role in controlling the particles size, controlling the morphology, dispersion as well as the activity of the synthesized nanomaterials[8-10]. Controlled and precise growth of nanoparticles with the desired shape and size can be tuned by altering the morphology of the support. Recently, porous substances with a high surface area like montmorillonite clay minerals, zeolites, charcoals containing nanosize channels etc. have been used for the stabilization of metal nanoparticles[12-19]. Due to stringent and growing environmental regulations, the chemical industry needs the development of eco-friendly and sustainable synthetic methods. Montmorillonite is environmentally benign, cheap, easily available alumino-silicate clay mineral of the smectite group. It exhibits some unique properties such as high cation exchange capacity, intercalation, swelling etc. which allow modifications of the structural properties by acid activation. Acid activated montmorillonite clay is partially delaminated and exhibits higher surface area containing both micro and mesopores, and can be utilized as a host for synthesis of metal nanoparticles in desired size and shape[16,18].

The heterogeneous metal nano-catalysts provide considerable advantages like easy isolation of products, efficient recovery and recyclability of catalysts. Moreover, in recent

years the strategy of magnetic separation of catalysts attracted much attention over filtration or centrifugation as it prevents the loss of catalyst[20-21]. Hence, Fe_3O_4 is extensively studied as a magnetically recoverable catalyst (MRC) for various organic transformations[22-26].

The Baeyer–Villiger oxidation is of considerable interest in organic chemistry because the products, lactones or esters, are important synthetic intermediates in the agrochemical, chemical and pharmaceutical industries[27-29]. A variety of carbonyl compounds, such as ketones, cyclic ketones, benzaldehydes and carboxylic acids can be transformed into various oxidised products, such as esters, lactones, phenols and anhydrides respectively through this reaction[30-31]. The oxidants used in the traditional Baeyer–Villiger oxidation are organic peroxy acids which potentially produce large amounts of harmful waste. Different types of homogeneous, heterogeneous, and enzyme catalysts are reported for the Baeyer–Villiger oxidation, and are often carried out with expensive, hazardous peracids, including *in-situ* generated organic peroxides formed from aldehydes and molecular oxygen, leading to the formation of one equivalent of the corresponding carboxylic acid[32-35]. Recent effort has led to the development of a greener heterogeneous catalytic system with hydrogen peroxide as the sole oxidant[36-42].

We report here, the synthesis of Fe_3O_4 magnetic nanoparticles supported montmorillonite clay (Fe_3O_4@AT-mont.) and their catalytic Baeyer-Villiger oxidation of cyclic and aromatic ketones using H_2O_2 as oxidants. The Fe_3O_4-nanoparticles serve as efficient green and heterogeneous catalyst for the oxidation of cyclic and aromatic ketones with excellent yields and selectivity under mild solvent free conditions. The advantages of this catalytic system are the, solvent free condition, low cost of the metal and magnatic separation of the catalyst. Moreover the catalyst can be reused several times without any significant loss in its catalytic activity.

2. Experimental

2.1. Materials and Methods

Bentonite (procured from Gujarat, India) containing quartz, iron oxide etc. as impurities was purified by sedimentation technique to collect the < 2 μm fraction. The basal spacing (d_{001}) of the air dried sample was about 12.5 Å. The surface area of the purified montmorillonite (mont.) was determined by N_2 adsorption analysis and found to be 101 m^2g^-^{1}. The analytical oxide composition of the bentonite determined was SiO_2: 49.42%; Al_2O_3: 20.02%; Fe_2O_3: 7.49%; MgO: 2.82%; CaO: 0.69%; loss on ignition (LOI): 17.51%; and others (Na_2O, K_2O and TiO_2): 2.05%.The purified mont. is then treated with 4 M hydrochloric acid so as to leach out the excess cations and increase the surface area. All operations were carried out under N_2 environment. H_2O_2 (30% w/v) and $CHCl_3$ (IR grade) were purchased from M/S Merck, Germany and used without further purification. $FeCl_3$, $NaBH_4$, cyclopentanone, cyclohexanone, cyclohex-2-ene-1-one, 2-methylcyclohexanone, 3-methylcyclohexanone, 4-methylcyclohexanone, cycloheptanone and cyclooctanone were purchased from sigma-Aldrich, USA and all reagents were used as supplied. Acetophenone, 4-methylacetophenone, 4-hydroxyacetophenone, 4-nitro acetophenone were purchased from Alfa Aesar, U.K. and were used as supplied.

Powder XRD spectra were recorded on a Rigaku, Ultima IV X-ray diffractometer of 2θ range 2-80° using Cu-Kα source (λ = 1.54 Å). Surface area, pore volume, average pore diameter were measured with the Autosorb-1 (Quantachrome USA). Surface areas of the samples were measured by adsorption of nitrogen gas at 77 K and applying the Branauer-Emmett-Teller (BET) calculation. Prior to adsorption, the samples were degassed at 250 ^{o}C for 3 h. Pore size distributions were derived from desorption isotherms using Barrett-Joyner-Halenda (BJH) method. Scanning electron microscopy (SEM) images and energy dispersive X-ray spectroscopy (EDX) were obtained with Leo 1430 vp operated at 3 and 10 kv. Prior to

examination, the samples were coated with gold. Transmission electron microscopy (TEM) and high resolution transmission electron microscopy (HRTEM) images were recorded on a JEOL JEM-2011 electron microscope and the specimens were prepared by dispersing powdered samples in isopropyl alcohol, placing them on a carbon coated copper grid and allowing them to dry. The Fe contents were determined by using Atomic Absorption Spectrometer (AAS), Perkin Elmer, AAnalyst-700 instrument. The reaction products were analyzed by GC (Chemito 8510, FID).

2.2. Preparation of support

Purified powdered mont. (8 g) was taken in a round bottom flask and 400 ml 4 M hydrochloric acid was added to it. The resulting dispersion was refluxed for 1 h. After cooling the supernatant liquid was discarded and the activated mont. was repeatedly centrifuged with deionised water till the pH of the water becomes nearly 7. The resulting mass was dried in an air oven at $50 \pm 5\ ^{\circ}C$ and designated as AT-mont.

2.3. Preparation of Fe_3O_4 magnetic nanoparticles suppoted on AT-mont.

1 g powdered AT-mont.was dispersed in 60 ml of double distilled water in a beaker and to it 9 mmol of $FeCl_3$ was added, which was then heated to about $60\ ^{\circ}C$. Few drops of 2 M NaOH solution was added to the mixture till precipitation starts and the mixture was allowed to stir at $60\ ^{\circ}C$ for 15 min. 10 ml aqueous solution of $NaBH_4$ (2 mmol) was added and the mixture was stirred for 30 min. A bar magnet is held at the bottom of the beaker and all the nanoparticles get sticked to the bottom and the aqueous part was poured out. Using this technique, the nanoparticles are repeatedly washed with distilled water and finally dried in a vacuum desiccator. The material was designated as Fe_3O_4@AT-mont.

2.4. Catalytic oxidation of ketones

Ketone (3 mmol), H_2O_2 [2 ml, 18 mmol (approx)] and 20 mg Fe_3O_4@AT-mont. were added and the reaction mixture was stirred at room temperature for 6 h. To study the

recyclability, the used catalyst was separated from the reaction mixture simply with a magnetic needle retriever. The separated catalyst was washed with acetone and dried in desiccators before using it in the subsequent run. The product which contains water as a byproduct was removed by using sodium sulphate. The conversion of the reaction were determined using GC.

3. Results and discussion

3.1. Characterization of Support

The parent mont. exhibited an intense basal reflection at 2θ value of 7.06° corresponding to a basal spacing of 12.5 Å in PXRD analyses [Fig. 1]. The intensity of basal reflection decreases considerably after 1 h acid activation, which implies that the layered structure of the clay is disrupted and also a low intense broad reflection of 2θ in the range 20–30° confirmed the formation of amorphorous silica[12]. The N_2-sorption type-IV isotherm with a H3 hysteresis loop at P/Po ~ 0.4–0.9 [Fig. 2] for AT-mont. confirms the presence of both both micro- and mesopores with an average pore diameters ~ 3.4 nm. AT-mont. posses high surface area up to 346 m^2 g^{-1} (surface area for parent mont. is 101 m^2g^{-1}) with pore volume of ~ 0.3 cm^3g^{-1} [Table 1]. The increase of the surface area as well as pore volume is due to the leaching of Al^{3+} from the clay matrix during acid activation forming a porous clay matrix. The differential volumes *versus* pore diameter plot [Fig. 2 (inset)] indicats a narrow pore size distribution. The SEM image of AT-mont. [Fig. 3(a)] showed the formation of pores on the clay surface. The EDX pattern of the surface [Fig. 3(b)] revealed the presence of predominant amounts of Si compared to Al on the surface. It therefore indicates the absence of Fe on the surface of the AT-mont.

3.2. Characterization of Fe_3O_4@AT-mont.

Powder XRD analysis of Fe_3O_4@AT-mont. [Fig. 4] shows six peaks at 2θ values 20.76, 30.16, 35.66, 43.08,57.06 and 62.6 due to the (111), (220), (311), (400), (511), (440) indices of face centered cubic (fcc) lattice of the Fe_3O_4 nanoparticles, which are indexed to

the spinel structure of pure stoichiometric Fe_3O_4 (JCPDS Card No. 19–0629)[43]. The BET surface area and total pore volume of Fe_3O_4@AT-mont. were found less compared to AT-mont [Table 1]. The appreciable decrease of the surface area and the pore volume after supporting Fe_3O_4 nanoparticles might be due to blocking of some of the pores by Fe_3O_4 nanoparticles. In addition, the presence of Fe_3O_4 nanoparticles may cause complexities in porosity measurement with nitrogen sorption, as the electrostatic forces between an adsorbate (*i.e.* nitrogen) and the metallic surface may affect the measured values to some extent. However, the increase of pore diameter may be due to rupture of some of the pore walls to generate bigger pore during the formation of the Fe_3O_4 nanoparticles and during catalytic reactions. The SEM-EDX analysis also confirms the presence of Fe_3O_4 nanoparticles on the surface of the AT-mont. [Fig. 5(a) & 5(b)] along with other elements of clay matrix. The elemental dot mapping [Fig. 6] clearly shows the homogeneous distribution of Fe throughout the support. The TEM images of Fe_3O_4@AT-mont. [Fig. 7] reveal that most of the Fe_3O_4 nanoparticles are dispersed on AT-mont. with average particle size around 10 nm. The XPS spectra [Fig. 8] of Fe_3O_4 gives two peaks at 710.8 eV and 724.2 eV, which are the characteristic of Fe $2P_{3/2}$ and Fe $2P_{1/2}$ respectively. On deconvolution of the XPS peaks show that the peak at 710.8 consists of two peaks at 709. 5 and 710.6 which are respectively for FeO and Fe_2O_3 components of Fe_3O_4[47]. The mean relative area of each constituent peak assigned to FeO and Fe_2O_3 is 32.28% and 67.72% respectively which is consistent with the theoretical ratio for Fe_3O_4 (FeO 33% and Fe_2O_3 67%). A very low intensity peak centered at 719 eV[44,45] is observed in the deconvoluted XPS spectrum [Fig. 8] indicating presence of negligible amount of γ-Fe_2O_3. The room temperature magnetization hysteresis curve of Fe_3O_4@AT-mont. [Fig. 9] shows saturation magnetization (Ms) of 55.01 emu g^{-1} with near zero remanence (Mr) and coercivity (Hc) confirmed its superparamagnetic nature[43,46]. The

Fe_3O_4@AT-mont. can be manipulated by an external magnet which is necessary for magnetic separation. The Fe content in 100 mg of Fe_3O_4@AT-mont. is found to be 33.3 mg.

3.3. Catalytic activity

The catalytic activity of the synthesized Fe_3O_4@AT-mont. was investigated towards the Baeyer–Villiger oxidation of different cyclic and aromatic ketones for different time periods, using hydrogen peroxide as the oxidizing agent at room temperature and good to excellent results were obtained. The highest conversion of 98 % was obtained after 6 h of stirring at room temperature [Table 2]. The catalytic activity was investigated towards the same reaction using water (2 ml) as only solvent, however no conversion was found. Therefore, H_2O_2 clearly stands out as the oxidizing agent of our choice by considering its high conversion rate, greener nature and environmental acceptability. To check the effect of the support, the reaction was also carried out using neat mont. and AT-mont. as catalysts without loading of Fe_3O_4 magnetic nanoparticles, but no conversion was observed.

The versatility and limitations of various substrates as well as the efficiency of the catalyst for Baeyer-Villiger oxidation of cyclic and aromatic ketones were studied. All the selected cyclic and aromatic ketones yield the desired ester with a considerably good conversion. In general, the cyclic ketones showed higher conversion than the aromatic ones. This may be due to the ring strain present in the cyclic ketones making them less stable than the aromatics. Moreover, the resonance effect present in the aromatic ketones may also be a factor for stabilizing them which is absent in the cyclic ones. The cyclic ketone i.e. cyclohexanone (Entry 2) showed the maximum conversion of 98 % to its corresponding ester i.e. caprolactone while the aromatic acetophenone (Entry 11) exhibited lower conversion of 88 % to the corresponding ester. A possible reaction pathway for the Baeyer-Villiger oxidation of ketone with H_2O_2 as oxidant is shown in scheme 1. The possible active site for the reaction is considered to be Fe(III), as in presence of H_2O_2, Fe(II) easily gets oxidized to

Fe(III)[47]. A comparison of different reported catalysts with the present work is shown in the Table 3. It is clear that the present catalyst shows a better catalytic activity.

The recyclability of the catalyst, Fe_3O_4@AT-mont., was investigated in the oxidation of cyclohexanone and acetophenone. The catalyst was separated from the reaction mixture simply with the help of a magnetic needle retriever [Fig. 10]. The recyclability results clearly indicate that the catalyst remained active without any significant loss in efficiency [Table 2]. The recovered catalyst was further investigated through N_2-sorption isotherm studies. The surface area of the recovered catalysts decrease to a certain extent compared to 186 m^2 g^{-1} of freshly prepared catalyst [Table 1]. The BJH pore size of the recovered catalysts increases to a certain extent as compared to the fresh catalyst [ESI Fig. 1]. The decrease of the surface area and the pore volume after catalytic runs is due to the raptures of some of the pore walls resulting bigger pores which reflects in the higher pore diameter value. The Fe content in the recovered catalyst after third run was estimated using AAS and found to be 30.1 mg per 100 mg of the catalyst, which is almost same as that of fresh catalyst. To check the heterogeneity, a filtration test was performed for entry 2. The reaction was allowed to run for three hour and then the catalyst was separated from the reaction mixture and again it was allowed to run without the catalyst for next four hour. It was found that the conversion after first three hour remained unchanged till the end of the reaction after separation of the catalyst. This confirms that, no leaching of any active species of the catalyst takes place during catalytic reaction.

4. Conclusion

The Fe_3O_4@AT-mont. composite has been synthesized by the *in-situ* generation of the Fe_3O_4 magnetic nanoparticles into the nanopores of modified montmorillonite clay and was characterized by PXRD, TEM, SEM-EDX, FTIR, XPS, VSM and Surface Area analysis. The average particle size of Fe_3O_4 nanoparticles was found to be around 10 nm and showed efficient catalytic activity for Baeyer–Villiger oxidation of various ketones to corresponding

products in the presence of hydrogen peroxide as an oxidant at room temperature under solvent free condition and exhibited conversion maximum up to 98 %. The catalyst was magnetically recovered and recycled for several runs without any significant loss of efficiency. The operational simplicity, easy magnetic recovery and low cost of the catalyst, as well as environmentally friendly reaction conditions, make it an attractive catalyst.

Acknowledgments

References

1. H. Goesmannand, C. Feldmann, Angew. Chem., Int. Ed., 2010, 49, 1362-1395.
2. C. N. R. Rao, G. U. Kulkarni, P. J. Thomas and P. P. Edwards, Chem. Soc. Rev., 2000, 29, 27-35.
3. Metal Nanoparticles: Synthesis, Characterization and Application, ed. D. L. Feldheim and C. A. Floss Jr, CRC Press, New York, 2002.
4. J. M. Campelo, D. Luna, R. Luque, J. M. Marinas and A. A. Romero, Chem Sus Chem, 2009, 2, 18-45.
5. A. C. Templeton, W. P. Wuelfing and R. W. Murray, Acc. Chem. Res., 2000, 33, 27-36.
6. D. Dutta, B. J. Borah, L. Saikia, M. G. Pathak, P. Sengupta and D. K. Dutta, Appl. Clay Sci., 2011, 53, 650-656.
7. G. Schmid and B. Corain, Eur. J. Inorg. Chem., 2003, 3081-3098.
8. B. J. Borah, D. Dutta and D. K. Dutta, Appl. Clay Sci., 2010, 49, 317–323.
9. J. D. Aiken and R. G. Finke, J. Am. Chem. Soc., 1999, 121, 8803–8810.

10. F. Schröder, D. Esken, M. Cokoja, M. W. E. van den Berg, O. I. Lebedev, G. V. Tendeloo, B. Walaszek, G. Buntkowsky, H. H. Limbach, B. Chaudret and R. A. Fischer, J. Am. Chem. Soc., 2008, 130, 6119–6130.

11. T. Tsukatani and H. Fujihara, Langmuir, 2005, 21, 12093–12095.

12. A. Phukan, J. N. Ganguli and D. K. Dutta, J. Mol. Catal.: A Chem., 2003, 202, 279-287.

13. O. S. Ahmed and D. K. Dutta, Langmuir, 2003, 19, 5540–5541.

14. O. S. Ahmed and D. K. Dutta, Thermochim. Acta, 2003, 395, 209–216.

15. P. B. Malla, P. Ravindranathan, S. Komarneni and R. Roy, Nature, 1991, 351, 555–557.

16. B. J. Borah, D. Dutta, P. P. Saikia, N. C. Barua and D. K. Dutta, Green Chem., 2011, 13, 3453–3460.

17. M. Bora, J. N. Ganguliand D. K. Dutta, Thermochim. Acta, 2000, 346, 169–175.

18. P. P. Sarmah and D. K. Dutta, Green Chem., 2012, 14, 1086–1093.

19. D. K. Dutta, D. Dutta, P. P. Sarmah, S. K. Bhorodwaj and B. J. Borah, J. Biomed. Nanotechnol., 2011, 7, 76–77.

20. V. Polshettiwar, B. Baruwati, R.S. Varma, Chem. Commun., 2009, 14, 1837–1839.

21. M.B. Gawande, P.S. Branco, R.S. Varma, Chem. Soc. Rev., 2013, 42, 3371–3393.

22. T. Zeng, W.-W. Chen, C.M. Cirtiu, A. Moores, G. Song, C.J. Li, Green Chem., 2010, 12, 570–573.

23. B. Sreedhar, A.S. Kumar, P.S. Reddy, Tetrahedron Lett., 2010, 51, 1891–1895.

24. M.M. Mojtahedi, M.S. Abaee, T. Alishiri, Tetrahedron Lett. 50 (2009) 2322–2325.

25. H. Firouzabadi, N. Iranpoor, M. Gholinejad, J. Hoseini, Adv. Synth. Catal., 2011, 353, 125–132.

26. X.J. Wu, R. Jiang, B. Wu, X.-M. Su, X.-P. Xu, S.-J. Ji, Adv. Synth. Catal., 2009, 351, 3150–3156.

27. G.R. Krow, Org. React., 1993, 43, 251-798.

28. A. Baeyer and V. Villiger, Ber. Dtsch. Chem. Ges., 1899, 32, 3625-3633.

29. A. Corma, L. T. Nemeth, M. Renz and S. Valencia, Nature, 2001, 412, 423-425.

30. T. Hara, M. Hatakeyama, A. Kim, N. Ichikuni and S. Shimazu, Green Chem., 2012, 14, 771–777.

31. C. Li, J. Wang, Z. Yang, Z. Hu, Z. Lei, Cat. Com., 2007, 8, 1202–1208.

32. R. Bernini, A. Coratti, G. Fabrizi, A. Goggiamani, G. Fabrizi, A. Goggiamani, Tetrahedron Lett., 2003, 44, 8991-8994.

33. G. Strukul, Angew. Chem., Int. Ed., 1998, 37, 1198-1209.

11

34. M. Renz and B. Meunier, Eur. J. Org. Chem., 1999, 737-750.

35. G.-J. ten Brink, I. W. C. E. Arends and R. A. Sheldon, Chem. Rev., 2004, 104, 4105-4124.

36. C. Jiménez-Sanchidrián and J. R. Ruiz, Tetrahedron, 2008, 64, 2011-2026.

37. A. Bhoumik, P. Kumar, R. Kumar, Catal. Lett., 1996, 40, 47-50.

38. U. R. Pillai, E. S.-Demessie, J. Mol. Catal.: A Chem., 2003, 191, 93–100.

39. Y. Imada, H. Iida, S. I. Murahashi, T. Naota, Angew. Chem. Int. Ed., 2005, 44, 1704 – 1706.

40. M. Renz, T. Blasco, A. Corma, V. Fornes, R. Jensen, L. Nemeth, Chem. Eur. J., 2002, 8, 4708-4717.

41. M. Paul, N. Pal, J. Mondal, M. Sasidharan, A. Bhaumik, Chem. Eng. Sci., 2012, 71, 564–572.

42. X. Zhang, J. Ye, L. Yu, X. Shi, M. Zhang, Q. Xu, M. Lautens, Adv. Synth. Catal., 2015, 357, 955–960.

43. G.H. Du, Z.L. Liu, X. Xia, Q. Chu, S.M. Zhang, J. Sol-Gel Sci. Technol., 2006, 39, 285–291.

44. S. Lian, Z. Kang, E. Wang, M. Jiang, C. Hu, L. Xu, Solid State Commun., 2003, 127, 605–608.

45. P. Li, E.Y. Jiang, H.L. Bai, J. Phys. D. Appl. Phys., 2011, 44, 7879-7882.

46. X. Huo, J. Liu, B. Wang, H. Zhang, Z. Yang, X. She, P. Xi, J. Mater. Chem., 2013, 1,651–656.

47. M. A. Voinov, J. O. S. Paga´n, E. Morrison, T. I. Smirnova, A. I. Smirnov, J. Am. Chem. Soc., 2011, 133, 35–41.

Figures:
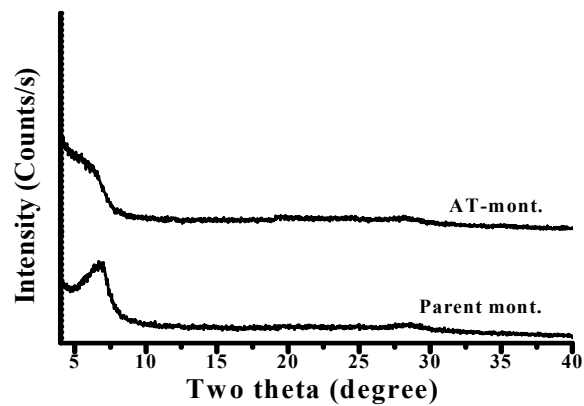
Fig. 1: Powder XRD of parent mont. and AT-mont.
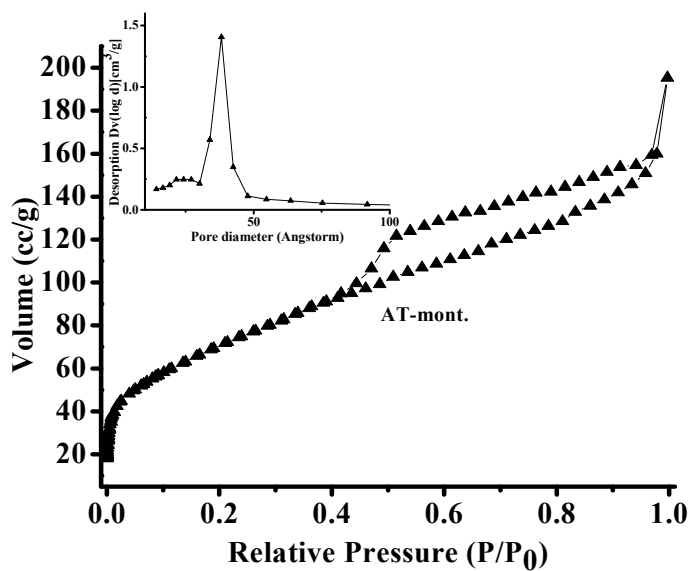
Fig. 2: BET isotherm and BJH pore distribution (inset) of AT-mont.
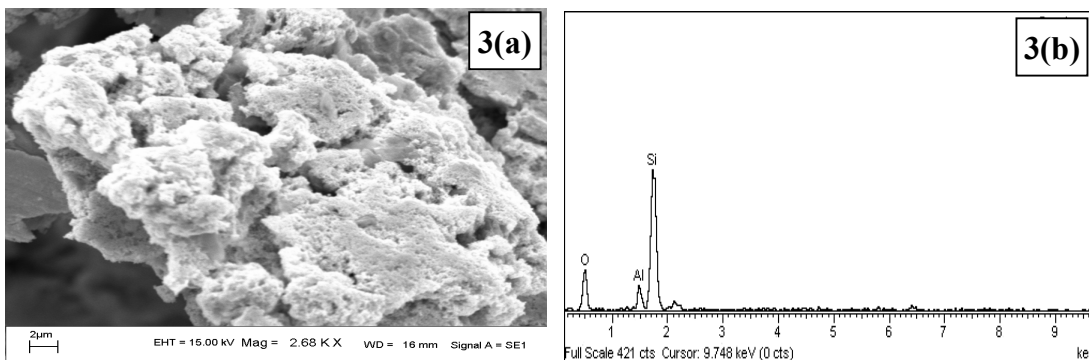
Fig. 3: (a) SEM image of AT-mont. **(b)** EDX spectra of AT-mont.
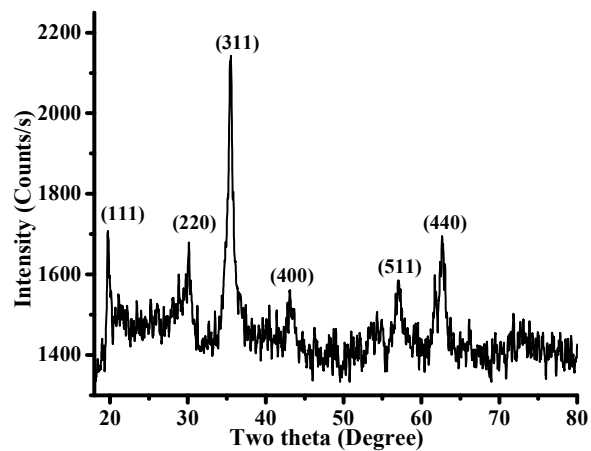
Fig. 4: Powder XRD pattern of Fe$_3$O$_4$@AT-mont.
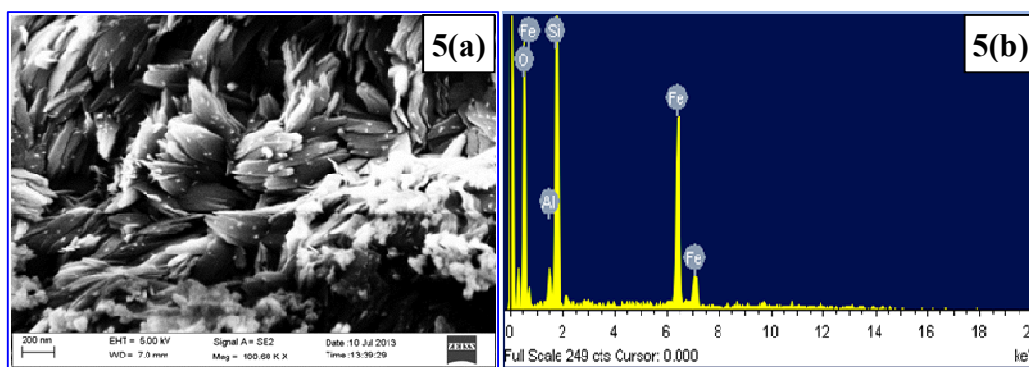
Fig. 5: (a) SEM image of Fe$_3$O$_4$@AT-mont., **(b)** EDX pattern of Fe$_3$O$_4$@AT-mont.
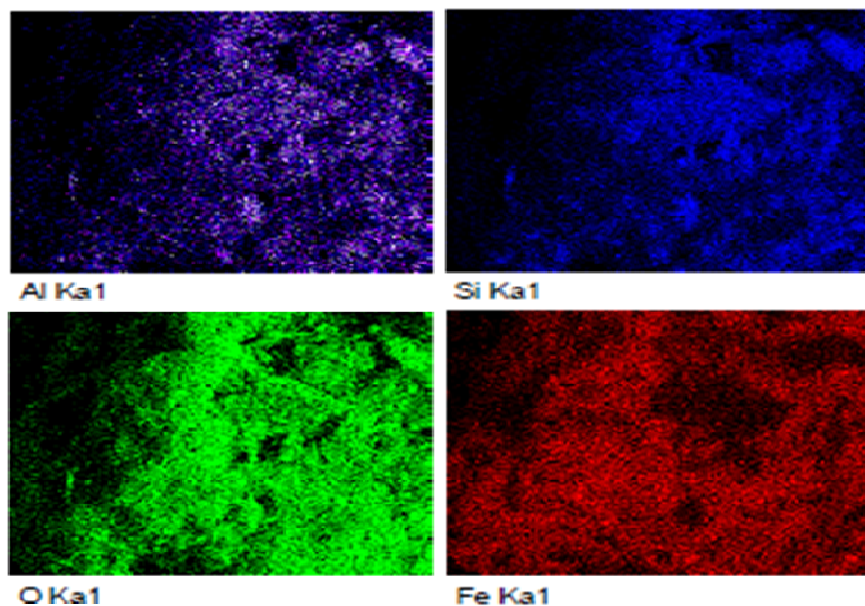
Fig. 6: Elemental dot mapping of Al, Si, O and Fe on Fe$_3$O$_4$@AT-mont. surface.
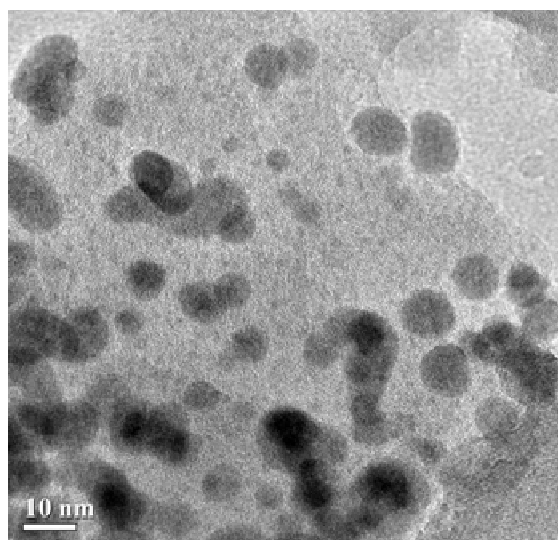
Fig. 7: TEM image of Fe_3O_4 nanoparticles on AT-mont.
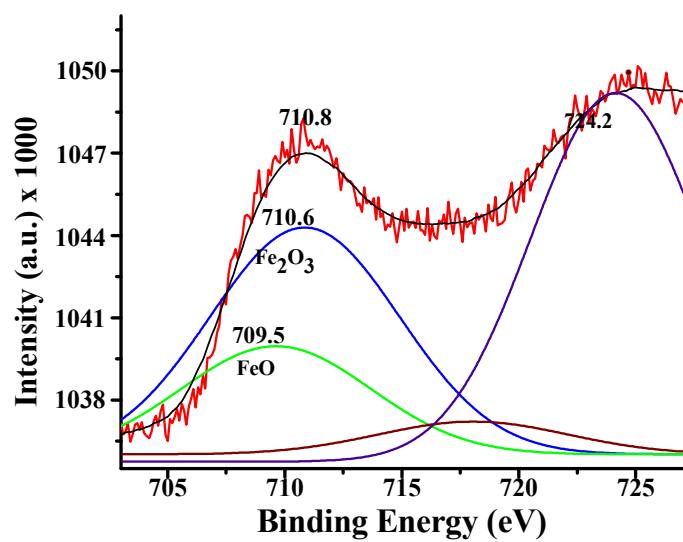
Fig. 8: XPS of Fe_3O_4@AT-mont. and results of deconvolution. (Red: experimental XPS spectrum; Black: best curve fit; Blue: $2P_{3/2}$ spectrum for Fe_2O_3; Green: spectrum for FeO, Brown: spectrum for γ-Fe_2O_3; Purple: $2P_{1/2}$ spectrum for Fe_3O_4)
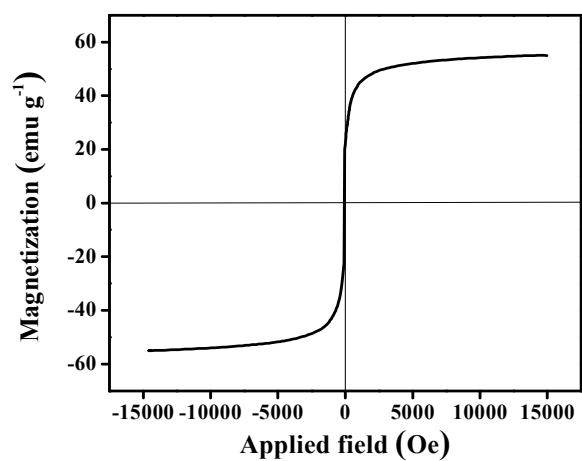
Fig. 9: Room temperature magnetization hysteresis curve of Fe_3O_4@AT-mont.
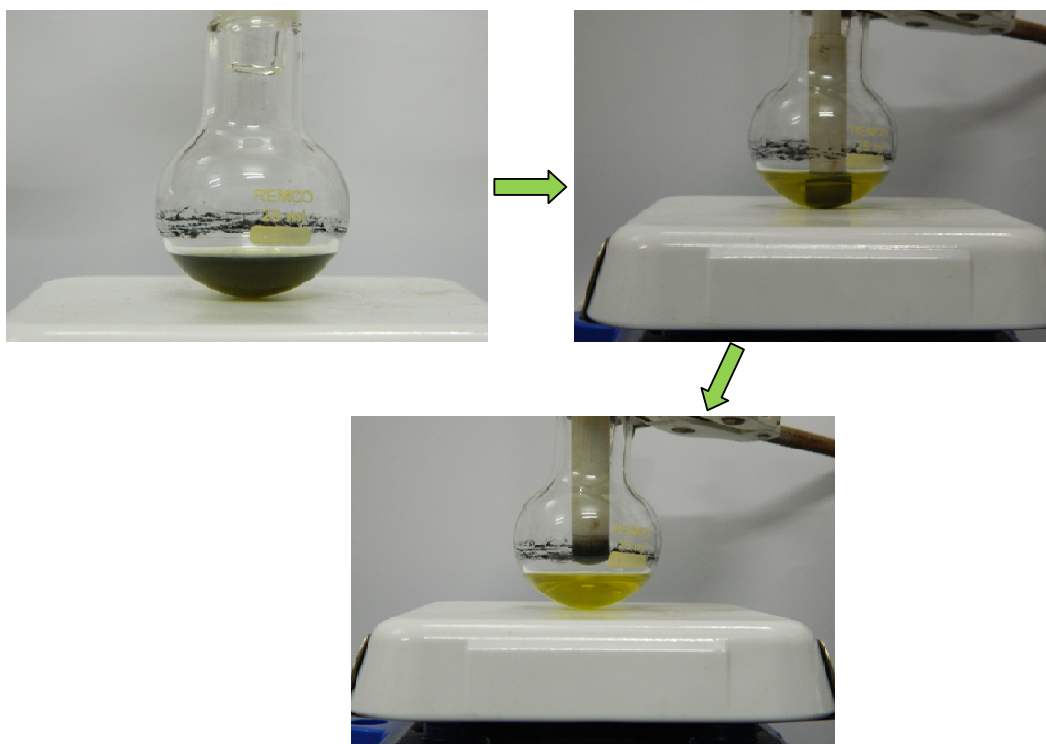
Fig. 10: Different steps showing the recovery of Fe_3O_4@AT-mont. catalyst after reaction using magnetic needle retriever.
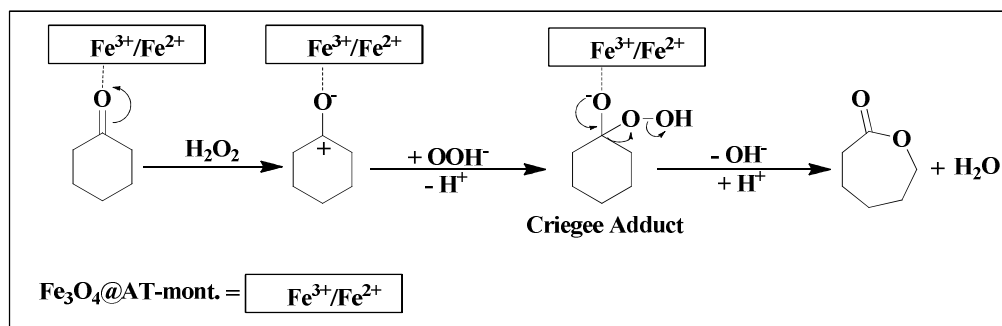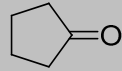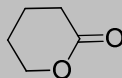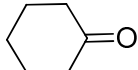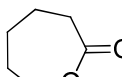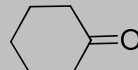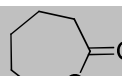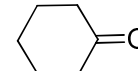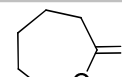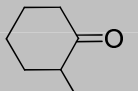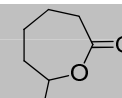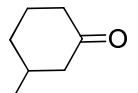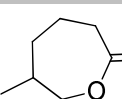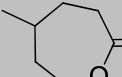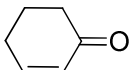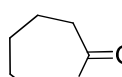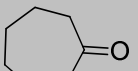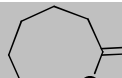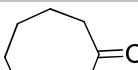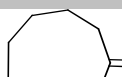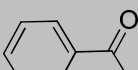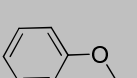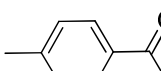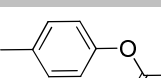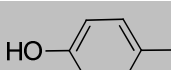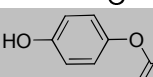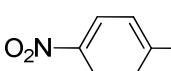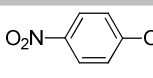
Scheme 1: A possible reaction path way for the Baeyer-Villiger Oxidation with H_2O_2 as oxidant.

Tables

Table 1. Surface properties of the AT-mont. and Fe_3O_4@AT-mont catalysts

|	Samples	Surface properties of support/catalysts		
		BET Surface area (m^2g^{-1})	Average pore diameter (nm)	Pore volume (cm^3g^{-1})
	AT-mont	346	3.4	0.3821
	Catalyst			
	After run Fresh ➜	186	4.8	0.3001
Fe_3O_4@AT-mont	1	166	6.5	0.2957
	2	124	9.5	0.2730
	3	124	12.2	0.2430

Table 2. Baeyer-Villieger Oxidation of cyclic and aromatic ketones using MRC, $Fe_3O_4@AT$-mont. under solvent free condition at room temperature.

Entry	Substrate	Product	Conversion (%)[a]	Selectivity (%)
1			86	100
2			98 (1st run) 96 (2nd run) 96 (3rd run) 94 (4th run)	100 100 100 100
3[b]			-	-
4[c]			-	-
5			83	90
6			80	92
7			84	94
8			77	96
9			77	97
10			76	98
11			88 (1st run) 85 (2nd run) 84 (3rd run) 84 (4th run)	90 90 90 90
12			84	88
13			75	87
14			77	85

Substrate:H_2O_2=1:6; [a] From GC analysis; [b] Parent mont. as catalyst; [c] AT-mont.as catalyst; Time 6 h.

Table 3: Comparison of the present catalyst with some reported catalyst for Baeyer- Villiger oxidation of ketones.

Sl. No.	Catalyst	Solvent	Oxidant	Temp. (^{o}C)	Time (h)	Conversion / Yield (max.)
1	[30]Sn-supported on clay	1,2-dichloroethane	H_2O_2	Refluxing temperature	2	100
2	[38]Sn exchanged hydrotalcites	acetonitrile	H_2O_2	70	4	58
3	[41]Mg-Al mixed oxide	1,4-dioxane	H_2O_2	70	12	88.7
4	[42]Oragnoselinium	acetonitrile	H_2O_2	Room temperature	24	92
5	Fe_3O_4@AT-mont. (present work)	Solvent free	H_2O_2	Room temperature	6	98

Graphical Abstract
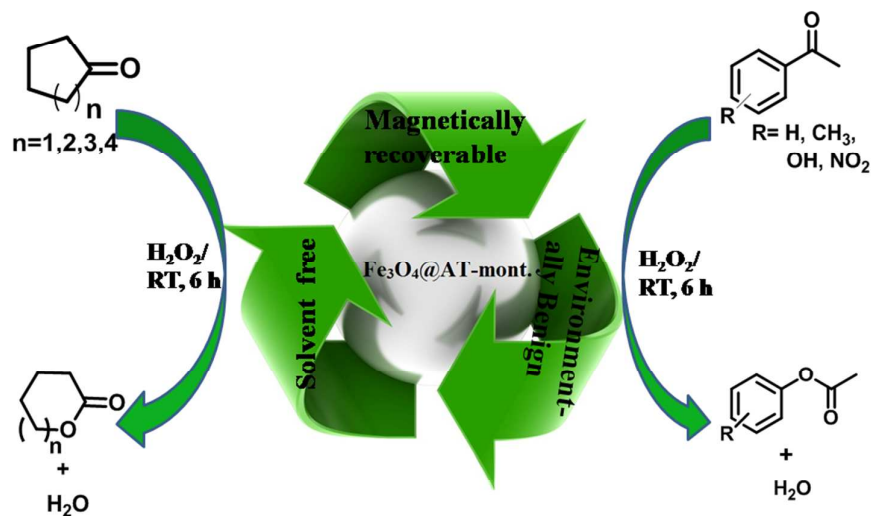
Fe$_3$O$_4$@AT-mont. based on naturally occurring montmorillonite exhibit efficient catalytic Baeyer-Villiger oxidation for different cyclic and aromatic ketones.